The structural role of in-plane interlocking in jack arches

V. Beatini, J.C.S. Clausen
Department of Civil and Architectural Engineering, Aarhus University, Aarhus, Denmark

D. Aita, E. Garavaglia
Department of Civil and Environmental Engineering (DICA), Politecnico di Milano, Milan, Italy

H. Caruso, L. Sgambi
Architecture, Built Environment, Université Catholique de Louvain, Tournai, Belgium

A. Pizzigoni
Independent scholar, formerly University of Bergamo, Bergamo, Italy

ABSTRACT: This paper explores how geometric variations in interlocking jack arches affect their failure modes and sensitivity to material parameters like strength and friction. The study employs and compares computational methods including Finite Element Analysis, graphical statics methods, and Discrete Element Modelling. The results show that interlocking features can reduce or eliminate the occurring of sliding collapse modes under self-weight. Collapse behaviour is independent of the material's compressive strength. Increased interlocking postpones failure also under support displacement, enhancing stress redistribution. These findings provide guidance for leveraging interlocking designs to improve structural efficiency and inspire innovative architecture. The study highlights the effectiveness of advanced computational methods in capturing both global and localized structural behaviour, offering robust and computationally efficient tools for analysis.

1 INTRODUCTION

Interlocking structures have a rich history, with varied forms implemented in jack arches dating back to ancient Egypt and throughout the Middle Ages in the Mediterranean region (Figure 1). These structures, once prevalent, have been largely abandoned and are now often considered architectural curiosities (Fournet, 2011) (Naby, 2014). As addressed in regards to topologically interlocking barrel vaults (Beatini and Tasora, 2022), it remains unclear whether these historical variations reflect a progressive understanding of structural behaviour or were influenced by factors such as a lack of shared knowledge, available skills, or suitable materials. Understanding these historical practices can inform modern design by revealing effective interlocking strategies that have withstood the test of time.

Interlocking blocks are those whose contact interface impedes their reciprocal motion under assumed motion directions and rigid boundaries (Estrin et al., 2011; Molotnikov et al., 2007). From a structural viewpoint, interlocking allows a masonry assembly to act more like a continuum under stress, preventing early disaggregation into constituent blocks. This advantage can enhance material efficiency (Tellia, 2018; Mousavian, Bagi, and Casapulla, 2022) and enable new design possibilities, such as arches with minimal horizontal thrust (Pizzigoni et al., 2024). Additionally, the crafting qualities of the elements, expressed through ancient and novel stereotomy, imbue the material artifact with intangible values (Aita et al. 2024; Pizzigoni, Beatini, and Paris, 2022), and enhanced sound absorption properties (Carlesso et al., 2012).

Despite these potential advantages, analysing interlocking blocks presents significant challenges. Physical testing, while effective, is resource-intensive (Molotnikov et al., 2015). Conventional digital analysis methods, such as those outlined in the Eurocode or standard Finite Element Method (FEM) based on homogenization techniques (macro modelling), are inadequate due to the complex geometry of interlocking interfaces. When the geometry of the blocks exceeds traditional design and construction practices, the assembly may become highly sensitive to subtle variations in design parameters like the friction coefficient, making accurate digital analyses essential (Aita et al., 2025).

Information Classification: General

This gap in efficient and accurate analysis methods limits the exploration and optimization of interlocking designs. There is a pressing need for advanced digital analysis tools that can accommodate complex geometries and help understand the role of each design variable in the structural performance of interlocking jack arches.

This study aims to establish relationships between specific features within the interlocking design and various loading scenarios, thereby providing insights into optimal design configurations. The objectives are to develop a digital analysis framework tailored for interlocking voussoirs in jack arches and identify significant design parameters for this typology under various possible boundary conditions.

To achieve the objectives, a set of computational modelling techniques that accurately capture the complex geometry of interlocking interfaces have been employed throughout the analyses and their results compared when feasible. The adoption of different approaches allows a mutual validation of the results by identifying critical modelling parameters, while the results touch different aspects related to the design criteria and the potential of such structures, contributing to broadening the knowledge of the same. For brevity, this paper presents the results of methods most pertinent to each parameter variation study. The latter include geometrical variations of the profiles of the blocks, material parameters like the friction coefficient and boundary conditions like support displacements.

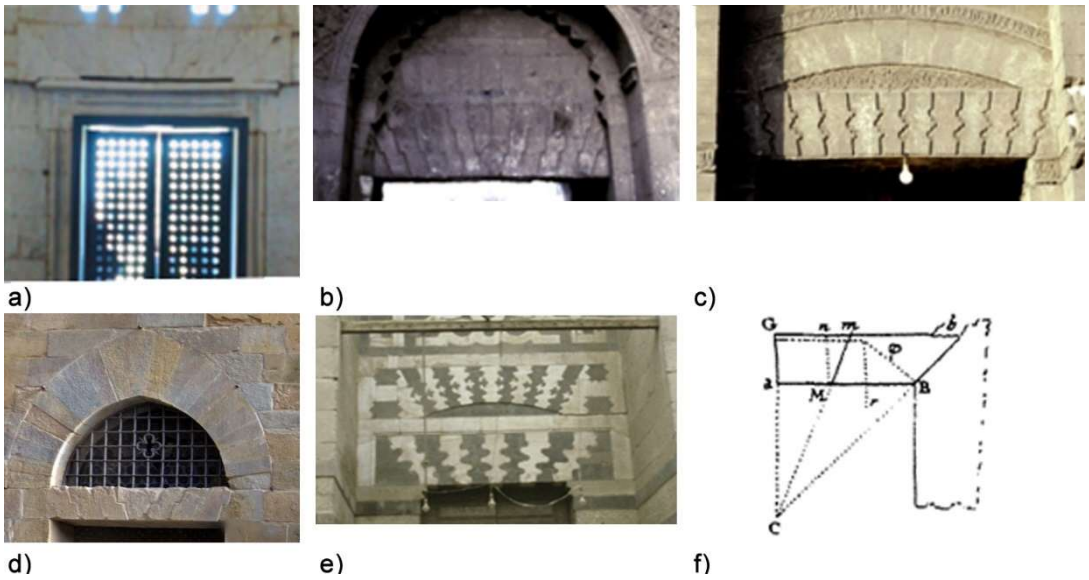


Figure 1 Ancient and historical interlocking jack arches. a) Mausoleum of Teodorico in Ravenna, VI CE b) The massive Bab al-Futuh (Conquest Gate) in the city walls of Cairo, XI CE (Allen, 2009) c) Mosque of al-Ṣāliḥ Ṭalā'iʿ, Cairo, XII (Allen, 2009), d) Palace of Bargello in Florence, XIII e) Madrasah and Khānaqāh of al-Zāhir Barqūq, Cairo XIV CE (Allen, 2009) f) The equilibrium of the flat arch according to Coulomb (1776).

2 MATERIALS AND METHODS

2.1 *Selection of design parameters*

Jack arches are typically structures used in masonry walls to allow the insertion of a door underneath. Because of this function, they usually have a limited span and, consequently, a limited number of blocks. The lack of structural sag limits the resisting moment arm that can be activated within the cross-section, which is compensated by the large depth of the blocks. Like traditional arches, their contact interfaces are typically inclined downward toward the centreline of the span to limit reciprocal sliding of the blocks and to work in compression, exploiting the high compressive strength of masonry. With reference to Figure 2, the geometry here investigated is a jack arch of span $B = 205.7$ cm composed of 7 blocks of typical width $b = 30$ cm, ($b' = 25.7$ cm), and height $H = 84$ cm. The blocks have therefore proportion $H/b = 2.8$. The out-of plane thickness

Information Classification: General

is assumed to be equal to 30 cm for all the jack arches. The lying angle to the horizontal is $\alpha = 98°$. In the third jack arch (Figure 2c), the horizontal segment of the step joint measures 7.5 cm.

From the examples in Figure 1, additional features in interlocking designs can include stepped or multi-step profiles, curved profiles, and profiles that are re-entrant or tapered toward the bottom. Due to their geometry, the collapse of jack arches always requires sliding to occur (Casapulla & D'Ayala, 2001). Historical treatises suggest that convergent profiles may instead exclude the possibility of a sliding failure to occur due to the equilibrium conditions compatible with a nil friction coefficient when the jack arch is subjected to its self-weight (Coulomb, 1776). Designs with re-entrant profiles, where the contact interfaces act as hinge-like constraints, can exhibit variations in failure modes, transitioning from sliding to bending with an increasing number of block (Dalaq & Barthelat, 2019). It is chosen thereof to consider substantial differences in the stereotomy of the blocks, to depict possible variation in failure mode. The study comprises three cases:

- Parallel-sided blocks (Figure 2a): the simplest case, serving as a baseline for comparison.
- Blocks with convergent sides (Figure 2b): where the sides of all the blocks taper towards the same point at the bottom.
- Blocks with a stepped profile (Figure 2c): incorporating a two-step interface between blocks.

The blocks are assumed to be made of a stone - like, compressive-only material with frictional interfaces. The material properties are density $\gamma = 2600$ kg/m^3, nil tensile strength and variable friction coefficient μ.

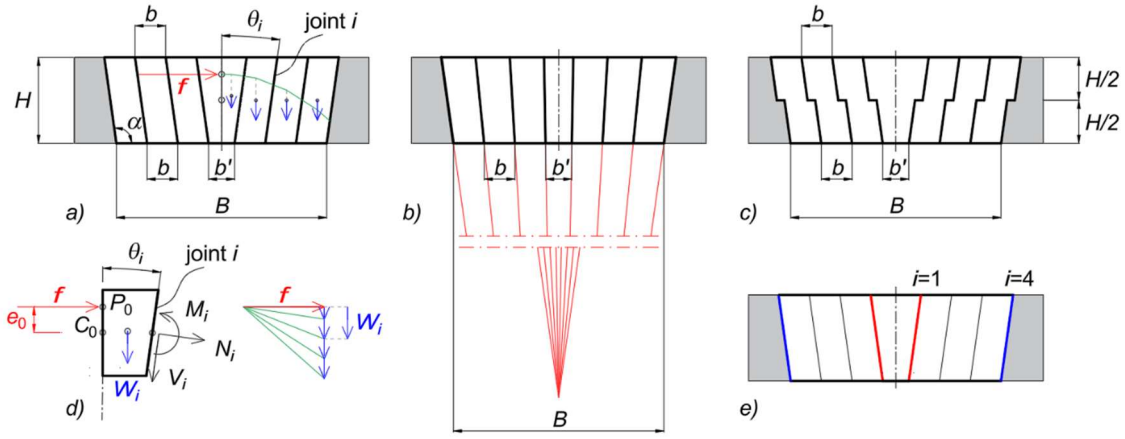


Figure 2 The jack arches models employed in the analyses distinguish by block designs with parallel (a), convergent (b) and stepped (c) joints. Equilibrium and force polygon of a portion of jack arch (d); anti-funicular polygon (a). Critical joints for the jack arch with parallel joints (e).

2.2 *Significant loading scenarios*

In addition to self-weight, useful to understand the general behaviour of the structure, significant analyses are derived from observing the organization of the remaining interlocking jack arches within the masonry wall. Often, these arches are further surmounted by a secondary arch that diverts away the load of the wall above, resulting subjected to their own self weight and possibly just a small imposed distributed load. This observation supports suggestions that interlocking was employed in ancient jack arches to increase the ability of masonry structures to resist displacement or subsidence (Camiz, 2015). Therefore, the behaviour under self-weight, increasing uniform gravity load, and support displacement is investigated and compared.

2.3 *Calibration of Analyses*

With reference to Table 1, the analyses performed are as follows. Finite Element Micro-Modelling captures the stress distribution within the individual blocks. The micro-modelling parameters include the material properties specified earlier, with the addition of an elasticity modulus of 54,000 MPa, and a Poisson's ratio of 0.2, under the assumption of linear elastic behaviour. Results

Information Classification: General

from this method are reported to validate the designs by evaluating whether excessive stress concentrations arise, and which material parameters need to be addressed by the successive analyses.

Graphical methods are typically used to identify critical thresholds and potential failure modes in a computationally efficient manner. Results from a variation of the Durand-Claye graphical method (Durand-Claye, 1867; Aita et al., 2019; Aita et al., 2025) are reported to investigate the role of the friction coefficient in the stability of the arch configurations. This method allows one to draw the so-called stability area, which provides the set of all the statically admissible solutions. This approach considers both friction and a limited compressive strength of the material. In the analyses here conducted, $\sigma_{ck} = 45$ MPa is set.

Discrete Element Modelling, specifically using Non-Smooth Contact Dynamics (NSCD), is particularly suitable for simulating the response of the structures under dynamic actions and the propagation of failure mechanisms (Beatini et al., 2018). The method assumes infinite compressive strength. In addition to the material parameters common to all cases, this method requires setting a cohesion value, here $c = 1e - 10$, which helps modelling the in-between behavior of masonry, sitting between associative and non-associative friction models (Aita et al., 2025). Analyses were performed in a custom ChronoEngine C++ formulation (Tasora et al., 2016) (Beatini et al., 2017). Here, results from simplified analyses of dynamic behaviour during support movement are reported, highlighting how interlocking features influence the overall stability under such conditions.

Table 1. Overview of proposed methods and main objectives

Method	**Core results**	**Insights**
Finite Element Analysis	Conditions for equilibrium Deformed configuration	Significant material parameters Deformability properties
Durand-Claye's graphical method	Conditions for equilibrium Variation of failure mode	Sensitivity to friction coefficient and to compressive strength
Non-Smooth Contact Dynamics	Dynamic behaviour and failure progression	Internal force distribution in relationship to geometry Associative/non-associative friction models

3 ANALYSES

3.1 *A finite element modelling for the jack arches*

The finite element modelling of the three jack arches was carried out using the ABAQUS software. The geometry of these structures was created in three dimensions using 10-node tetrahedral finite elements (C3D10) that employ quadratic interpolation functions. For the material, a linear elastic behaviour was considered (see the parameters specified in Section 2.3). The blocks were modelled separately, and their connection was simulated through a contact interaction. This interaction was implemented by considering a 'hard' contact in the normal direction to the contact surfaces, allowing the surfaces to separate during the load history. In the tangential direction, sliding was allowed by applying a frictional contact, controlled by a friction coefficient μ.

For the three jack arches, static analyses were performed by progressively diminishing the friction coefficient to find the minimum values of μ needed to ensure equilibrium under gravitational load (self-weight). For the first flat arch (parallel joints), this coefficient was determined to be 0.0982; for the second one (convergent joints), 0.0003; while the third one achieved equilibrium even when the coefficient μ was zero. Figure 3 shows the equilibrium positions of the segments

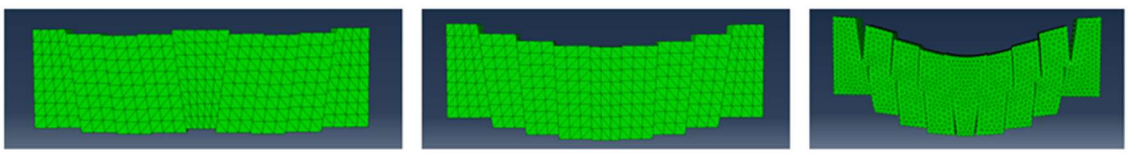


Figure 3 Displacements and deformations for the three flat arches in the equilibrium configuration with the minimum friction coefficient.

in the deformed state at the end of their respective analyses to find the minimum friction

Information Classification: General

coefficient. Given the varying degrees of deformability due to differing joint geometries, each image was reproduced with a different scale factor to enhance the visibility of segment displacements. The displacements and deformations of the first flat arch (Figure 3a) are amplified by 500 times, those of the second by 5000 times (Figure 3b), and those of the third by 100,000 times (Figure 3c).

It is interesting to observe that, for the first jack arch (Figure 3a), a downward sliding mechanism develops between the two lateral portions, each composed of three blocks. Additionally, mutual sliding occurs between the central segment and the lateral portions. For the second jack arch, a downward sliding is observed between the blocks, attributed to the deformability of the material; if the material were rigid, this mechanism would not be kinematically admissible. For the third jack arch, the deformed shape involves mutual rotation between the voussoirs.

3.2 *Analyses under gravitational loads: the 'stability area' method*

A modern version of Durand-Claye's method was applied to the three jack arches under self-weight to derive the minimum friction coefficient compatible with equilibrium and compare the results with those presented in Section 3.1.

Statically admissible solutions were calculated by considering the equilibrium conditions for the part of the structure between the ideal vertical midspan section and a generic joint i, whose inclination with respect to the vertical axis is defined by angle θ_i (see Figure 2a). These solutions also accounted for the strength and friction requirements of any cross-section i. Due to symmetry, an eccentric horizontal thrust f, ideally acts on the vertical crown section (see Figure 2d). The eccentricity of f with respect to the centroid, C_0, of the vertical section is denoted by e_0. The stability area represents the locus of points in the (f, e_0) plane corresponding to statically admissible solutions (Figure 4). After deriving the bending moment, M_i, and the normal force, N_i (Figure 2d), also the formal expressions for the limit bending moment, M_i^{lim}, dependent on the limited compressive strength of the material, and the minimum and maximum values of the thrust compatible with the friction coefficient (f_i^{sl+} and f_i^{sl-}, respectively) can be written. The intersection between the rotational domain A^{rot} (the yellow region in Figure 4a) and the sliding domain A^{sl} (the dashed region) yields the stability area A, see the yellow, dashed region of the (f, e_0) plane. By starting from the (infinite) statically admissible solutions (f, e_0) belonging to A, the corresponding force polygon and anti-funicular polygon can be easily traced for each of them (see as an example, Fig. 2d, right, and Fig. 2a). For further details, the interested reader is referred to (Aita et al., 2019; 2025). The incipient collapse condition, if present, is identified by progressively decreasing the friction coefficient as that corresponding to the vanishing of the stability area, i.e., when the sliding domain A^{sl} is reduced to a segment identified by the condition $\max_i f_i^{sl-} = \min_i f_i^{sl}$.

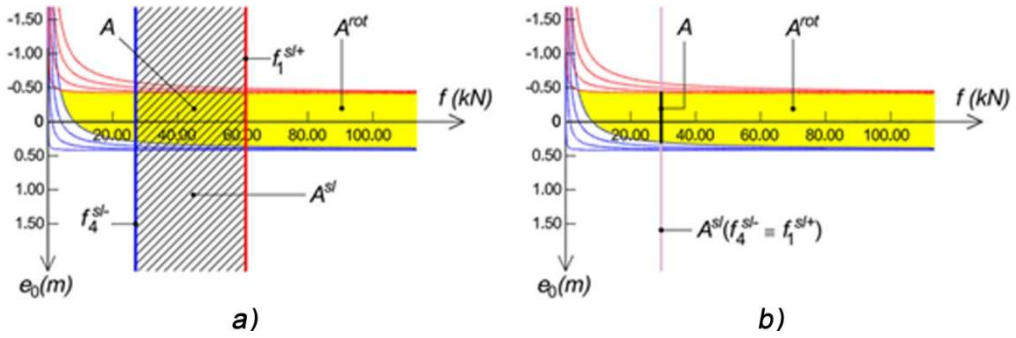


Figure 4 Examples of stability area related to the jack arch with parallel joints. Stability area for $\mu = 0.12$ (a). Stability area at the incipient collapse condition, $\mu = 0.098218$.

The stability area at incipient collapse related to the flat arch with parallel joints, see Figure 2a, is plotted in Figure 4b: in this case $\max_i f_i^{sl-} = f_4^{sl} = \min_i f_i^{sl} = f_1^{sl}$ for $\mu = 0.098218$, which matches sliding at the blue and red joints in Figure 2e, confirming the collapse behaviour as well as the limit value of the friction coefficient identified by the FEM, see Figure 3a. For the second

Information Classification: General

flat arch (Figure 2b) the limit equilibrium condition is attained when $\mu = 0$. In this case, $\max_i f_i^{sl-} = \min_i f_i^{sl+}$ at each joint, see also Coulomb (1776). For the third flat arch, equilibrium is possible even for $\mu = 0$, since sliding downwards is not admitted by the shape of the joints.

3.3 *Supports displacement*

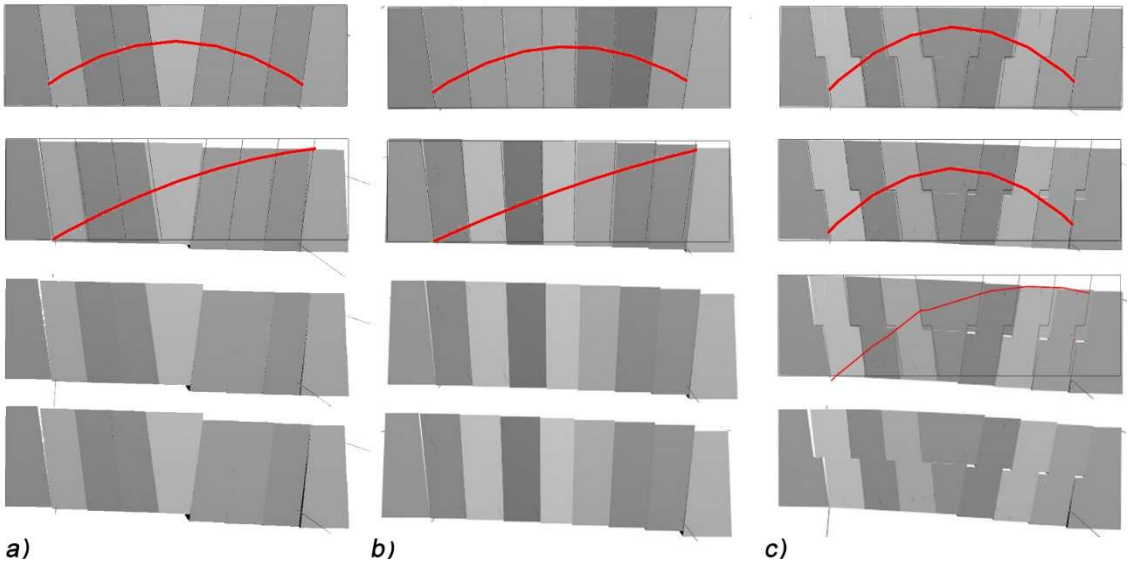


Figure 5 Snapshots from a simplified simulation of a downward displacing support, plotted at null displacement (1.5 s), d= 7.4 cm (51 s), d= 11.1 cm (75 s) and d= 14.8 cm (100 s), for the parallel (a), convergent (b) and stepped (c) models. The first displacement states are plotted alongside the thrust line derived from postprocessing the resultant contact forces in a parametric environment.

To capture the block-by-block interaction under large displacements, the NSCD approach mentioned in Section 2 was employed. Simulations were performed imposing a vertical downward displacement of 0.015 mm / s^{-2} to the centroid of the right end block. Because this imposed displacement (a non-modifiable boundary condition) could otherwise interfere with the solver's initial setup, it was delayed until 1.5 s of simulation time. The solver automatically computes the contact envelope by applying a small initial perturbation, so postponing the displacement ensures that the structure reaches equilibrium before the boundary condition is applied. Figure 5 illustrates snapshots from the simulation at various stages: at null displacement (1.5 s), $d = 7.4$ cm (51 s), $d = 11.1$ cm (75 s) and $d = 14.8$ cm (100 s). For lower displacement levels, the figure also includes the thrust line (funicular polygon) derived from postprocessing the resulting contact forces over the original position of the blocks (outlined in the background).

The results indicate notable differences in the structural response of the three jack arches. That with parallel joints (Figure 5a) splits into two subparts, demonstrating a poor capacity to activate a resistance mechanism, and fails due to sliding even at low displacement levels. As confirmed by the plot of the thrust line, any arch-like action is lost at $d = 7.5$ cm also for the jack arch with convergent joints (Figure 5b), However, this structure shows a more stepped failure mode, and visible failure effects are delayed, indicating a higher capacity to resist smaller displacements compared to the to the first jack arch. The flat arch with stepped joints (Figure 5c) demonstrates a significant capacity to adapt to the sliding support condition. At $d = 7.5$ cm it remains fully capable of activating an arch action. With further displacement, the blocks rotate noticeably away from the left support, eventually leading to failure. To contextualize these results, it is important to note that standard multi-ring masonry arches composed of a similar number of blocks do not exhibit such stress redistribution unless shear transfer mechanisms are implemented; typically, only the lower arch is involved in the resistance mechanism (Beatini et al., 2019; Nela et al., 2023).

Information Classification: General

4 CONCLUSIONS

This paper explored how key geometrical differences in interlocking jack arch designs influence their failure modes and sensitivity to material parameters like friction. The jack arches' behaviour under self-weight and support displacement was examined using multiple computational methods.

The results indicate that interlocking features can significantly reduce or even eliminate the dependence of collapse on a low friction coefficient under self-weight. As revealed by the graphic statics analysis, the collapse response is independent of the material's compressive strength, making the solution robust against variations in material properties. The FEA analyses show that employing a stepped profile limits free sliding of the blocks once sliding begins. The NSCD results for the case of support displacement confirm that higher levels of interlocking enable a transition from localized block responses to unified static and dynamic behaviour, which is an indication of enhanced structural performance (Foraboschi, 2019).

The illustrated methods effectively visualize both the global static and dynamic behaviour and the contribution of localized structural responses. It should be noted that, while some methods can be used effectively in more than one of the analyses performed, employing different approaches allows us to address the model's sensitivity to various parameters (e.g., friction coefficient or geometry) in a computationally efficient and readily interpretable manner—ultimately making the results more accessible to a broader audience. This approach not only provides a comprehensive understanding of structural behaviour highlighting the potential of such structures, but also it contributes to broadening the knowledge of the same. The findings can guide architects and engineers in leveraging interlocking features to enhance structural performance and inspire innovative architectural designs. Future studies should explore additional design details, such as curved block profiles, and investigate the interaction between jack arches and the masonry wall structure.

REFERENCES

Aita, D, Barsotti & R, Bennati, S. 2019. Looking at the collapse modes of circular and pointed masonry arches through the lens of Durand-Claye's stability area method. *Archive of Applied Mechanics* 89: 1537-1554. https://doi.org/10.1007/s00419-019-01526-z

Aita, D., Beatini, V., Caruso, H., Garavaglia, E. & Sgambi, L., 2025. Some remarks on non-standard behaviour with Coulomb's friction starting from an unconventional stone flat arch. *Engineering Structures* 326: 119539. https://doi.org/10.1016/j.engstruct.2024.119539

Aita, D., Beatini, V., Garavaglia, E., Paris, V., Pizzigoni, A. & Sgambi, L., 2024. The roofing system of the tholos of Athena Pronaia in Delphi: archaeological hypotheses and structural suggestions. *International Journal of Architectural Heritage,* 1–26. https://doi.org/10.1080/15583058.2024.2316289

Allen, T., 2009. *Constructs of Symmetry in Islamic Art*. Solipsist Press, Occidental, California.

Beatini, V., Royer-Carfagni, G. & Tasora, A., 2019. Modeling the shear failure of segmental arches. *International Journal of Solids and Structures* 158, 21–39. https://doi.org/10.1016/j.ijsolstr.2018.08.023

Beatini, V., Royer-Carfagni, G. & Tasora, A., 2018. The role of frictional contact of constituent blocks on the stability of masonry domes. *Proc. R. Soc. A*. 474, 20170740. https://doi.org/10.1098/rspa.2017.0740

Beatini, V., Royer-Carfagni, G. & Tasora, A., 2017. A regularized non-smooth contact dynamics approach for architectural masonry structures. *Computers & Structures* 187, 88–100. https://doi.org/10.1016/j.compstruc.2017.02.002

Beatini, V. & Tasora, A., 2022. Early experimentations within the masonry barrel vault. In Behnejad , SA, Parke, GAR, & Samavati, O (2022). Inspiring the Next Generation-Proc. *Int. Conf.Spatial Structures* 2020/21 (IASS2020/21-Surrey7). Inspiring the Next Generation, 3590.

Camiz, A., 2015. Morphology of Roman, Islamic and Medieval seismic design: pointed arch and ablaq. *Key Engineering Materials* 628, 9–14. doi:10.4028/www.scientific.net/KEM.628.9

Carlesso, M., Molotnikov, A., Krause, T., Tushtev, K., Kroll, S., Rezwan, K. & Estrin, Y., 2012. Enhancement of sound absorption properties using topologically interlocked elements. *Scripta Materialia* 66, 483–486. https://doi.org/10.1016/j.scriptamat.2011.12.022

Information Classification: General

Casapulla, C., & D'Ayala, D. 2001 Lower bound approach to the limit analysis of 3D vaulted block masonry structures. In *Computer Methods in Structural Masonry*, 5, 177-183. Computers & Geotechnics Ltd.

Coulomb, C. 1776. Essai sur une application de règles de maximis et minimis à quelques problèmes de Statique, relatifs à l'Architecture. *Mémoires de Mathématique et de Physique présentés a l'Académie Royale des Sciences, par divers Savans, et lûs dans les Assemblées, année 1773* 17: 343-382.

Dalaq, A.S. & Barthelat, F., 2019. Strength and stability in architectured spine-like segmented structures. *International Journal of Solids and Structures* 171, 146–157. https://doi.org/10.1016/j.ijsolstr.2019.04.012

Durand-Claye, A. 1867. Note sur la vérification de la stabilité des voûtes en maçonnerie et sur l'emploi des courbes de pression. *Annales des Ponts et Chaussées* 13: 63-93.

Estrin, Y., Dyskin, A.V. & Pasternak, E., 2011. Topological interlocking as a material design concept. *Materials Science and Engineering*: C 31, 1189–1194. https://doi.org/10.1016/j.msec.2010.11.011

Foraboschi, P., 2019. Masonry does not limit itself to only one structural material: Interlocked masonry versus cohesive masonry. *Journal of Building Engineering* 26. 1-14 https://doi.org/10.1016/j.jobe.2019.100831

Fournet, T., 2011. Trois Curiosités Architecturales Des Bains De Taposiris Magna (Égypte): Voûte À Crossettes, Radiateur et dalle Clavée. *Revue Archéologique* 323–347. https://doi.org/10.3917/arch.112.0323) .

Molotnikov, A., Estrin, Y., Dyskin, A.V., Pasternak, E. & Kanel-Belov, A.J., 2007. Percolation mechanism of failure of a planar assembly of interlocked osteomorphic elements. *Engineering Fracture Mechanics* 74, 1222–1232. https://doi.org/10.1016/j.engfracmech.2006.07.012

Molotnikov, A., Gerbrand, R., Qi, Y., Simon, G.P. & Estrin, Y., 2015. Design of responsive materials using topologically interlocked elements. *Smart Mater. Struct.* 24, 025034. https://doi.org/10.1088/0964-1726/24/2/025034

Mousavian, E., Bagi, K. & Casapulla, C., 2022. Interlocking joint shape optimization for structurally informed design of block assemblages. *Journal of Computational Design and Engineering* 9, 1279–1297. https://doi.org/10.1093/jcde/qwac054

Naby, H.M.S.A., 2014. The Treatment of the Architectural Unit above Openings of the Mamluk and Ottoman Facades in Cairo. *Journal of Islamic Architecture* 3, 82–93. https://doi.org/10.18860/jia.v3i2.2541

Nela, B., Pingaro, M., Trovalusci, P. & Pasca, M., 2023. Limit analysis of multi-ring masonry arches: a parametric study on the effects of friction angle, geometry, interlocking, and ring number. *Frontiers in Built Environment* 9, 1309696.

Pizzigoni, A., Beatini, V. & Paris, V., 2022. The Stone Roof Marble Tholos Tiles in the Sanctuary of Athena Pronaia at Delphi. Stereotomy and compression resistant forms in the domed roof structures of ancient Greece. *Structural* 240, 1–30. https://doi.org/10.5194/isprs-archives-XLVIII-M-2-2023-59-2023

Pizzigoni, A., Beatini, V., Paris, V., Beghini, A., Ferrari, R., Cocchetti, G. & Rizzi, E., 2024. Fornix: the circular platform-frame. *Proc*. IASS 2024 *Symposium. Redefining the Art of Structural Design*, International Association Space Structures (IASS), Zurich.

Tasora, A., Serban, R., Mazhar, H., Pazouki, A., Melanz, D., Fleischmann, J., Taylor, M., Sugiyama, H. & Negrut, D., 2016. Chrono: An Open-Source Multi-physics Dynamics Engine, in: Kozubek, T., Blaheta, R., Šístek, J., Rozložník, M., Čermák, M. (Eds.), *High Performance Computing in Science and Engineering, Lecture Notes in Computer Science*. Springer International Publishing, Cham, pp. 19–49. https://doi.org/10.1007/978-3-319-40361-8_2

Tellia, F., 2018. Stereotomy and Architectural Design at Foster+ Partners. *Nexus Network Journal* 20, 605–626. https://doi.org/10.1007/s00004-018-0380-1

Information Classification: General